Combined Circuit Model to Simulate Post-Quench Behaviors of No-Insulation HTS Coil

Mincheol Cho, So Noguchi, Jeseok Bang, Jaemin Kim, Uijong Bong, Jung Tae Lee, Soo Bin An, Kabindra R. Bhattarai, Kwangmin Kim, Kwanglok Kim, Chaemin Im, Ki Jin Han, and Seungyong Hahn

***Abstract*—This paper presents a "combined" circuit model to simulate non-linear behaviors of a no-insulation (NI) high temperature superconductor (HTS) coil. The key idea is a *selective* use of either the lumped circuit model or distributed depending on an operating condition. When the NI coil current is below its critical current, the radial leak currents through turn-to-turn contacts may be assumed to be uniformly distributed over the entire coil, thus, the lumped circuit model may suffice to analyze the NI behaviors. When the coil current increases beyond the critical current, the distributed model plays the role to simulate the spatial distribution of currents, both radial and azimuthal. By limiting the use of the time-consuming distributed model only for the post-quench part, the combined model enables substantial reduction in calculation time without sacrificing simulation accuracy. To verify the validity of the combined model, an over-current charging test of an NI HTS coil was simulated with the lumped, distributed, and combined models. The simulation results of the combined model are barely discernible from those of the distributed model, and agreed well with the measured ones as well. The results validate the combined model for more efficient simulation of an NI HTS coil.**

***Index Terms*—Combined model, distributed network model, equal power constraint, lumped circuit model, no-insulation.**

I. Introduction

NOTABLE progress has been made in the no-insulation (NI) high temperature superconductor (HTS) winding technique, since its first publication in 2011 [1]. To date, multiple NI HTS magnets have been designed and constructed, and most of them reached their target fields without experiencing electric burn-out upon a quench [1]–[13]. Recently mechanical damages of some high field NI HTS magnets were reported mainly due to large "over-currents" induced in electromagnetically coupled subcoils during a quench and consequent excessive magnetic stress [14]. Obviously, a good simulation approach to precisely analyze the non-linear behaviors of an NI HTS magnet is crucial to design and operate the magnet.

To date two kinds of numerical approaches have been reported to simulate the NI behaviors of a single coil [15]–[21] or even a *multi-coil* magnet [22]–[25]. The first approach is called lumped circuit model, initially reported in [1], where an NI coil is modeled with an inductor and a resister connected in parallel. Wang *et al.* [26], improved the initial lumped model with the *index resistance* incorporated to simulate transient behaviors of an NI coil more accurately. Bhattarai *et al.*, reported the first "magnet-level" lumped circuit analysis of an *actual* 7 T 78 mm NI all-REBCO magnet [22]. The second approach is called distributed network model, firstly reported in 2014 by Yanagisawa *et al.* [17], where an NI REBCO coil was subdivided into multiple segments and each segment was modeled with an individual lumped circuit model. Wang and Noguchi *et al.*, reported a similar model based on the partial element equivalent circuit (PEEC) technique [19]. Wang *et al.*, combined a thermal analysis based on the finite element method with the distributed network magnetic field analysis of an NI coil [18]. Magnet-level distributed network models were also reported by Markiewicz *et al.* [24] and Song *et al.* [25], separately, though application of the distributed model to *actual* NI HTS magnets has not been reported yet.

Both lumped and distributed models have pros and cons. The lumped model enables *fast* simulation but in limited accuracy particularly for the post-quench analysis, where the local distribution of quench currents in an NI coil is important. The distributed model enables simulation of the spatial distribution of currents upon a quench but it often takes days to simulate a single coil or even weeks a multi-coil magnet. This paper presents a "combined" approach, where either the lumped model or the distributed model is *selectively* used depending on an operating condition to take advantage of both models. First, details on the combined approach will be presented and followed by a case study to simulate an actual NI REBCO test coil [1]. Last, simulation accuracy of the combined model will be discussed at the end.

II. Conventional Approach: Lumped Circuit Model and Distributed Network Circuit Model

A. *Conventional Approach #1: Lumped Circuit Model*

Figure 1(a) shows a typical configuration of the lumped circuit model that consists of: (1) an inductor L_{coil} that represents

Manuscript received October 30, 2018; accepted February 2, 2019. Date of publication February 18, 2019; date of current version March 27, 2019. This work was supported by Samsung Research Funding & Incubation Center of Samsung Electronics under Project SRFC-IT1801-09. *(Corresponding authors: Seungyong Hahn and Ki Jin Han.)*

M. Cho, J. Bang, J. Kim, U. Bong, J. T. Lee, S. B. An, C. Im, and S. Hahn are with the Department of Electrical and Computer Engineering, Seoul National University, Seoul 08826, South Korea (e-mail: hahnsy@snu.ac.kr).

S. Noguchi is with the Graduate School of Information Science and Technology, Hokkaido University, Sapporo 060-0814, Japan (e-mail: noguchi@ssi.ist.hokudai.ac.jp).

K. R. Bhattarai, Kwangmin Kim, and Kwanglok Kim are with the National High Magnetic Field Laboratory, Tallahassee, FL 32310 USA (e-mail: kwangmin.kim@asc.magnet.fsu.edu).

K. J. Han is with the Division of Electronics and Electrical Engineering, Dongguk University, Seoul 04620, South Korea (e-mail: kjhan@dongguk.edu).

Color versions of one or more of the figures in this paper are available online at http://ieeexplore.ieee.org.

Digital Object Identifier 10.1109/TASC.2019.2899501

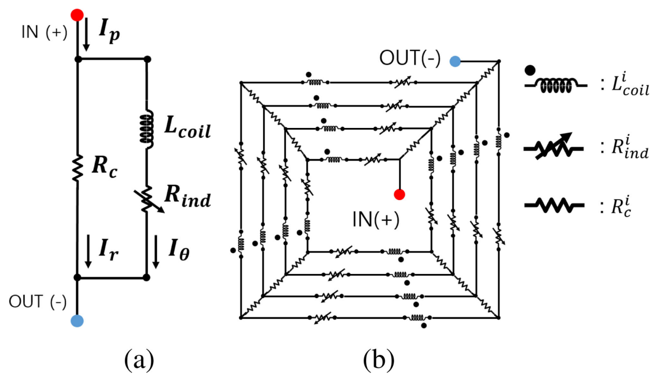

Fig. 1. (a) lumped circuit model, where L_{coil}, R_c, and R_{ind} are, respectively, coil inductance, characteristic resistance representing the radial current path through turn-to-turn contacts, and the index resistance; (b) distributed network model, where an NI coil is subdivided into multiple segments. Electrical components for each segment in the distributed model are similar to those in the lumped model: L^i_{coil} for inductance of the i^{th} coil segment, R^i_c characteristic resistance, and R^i_{ind} index resistance.

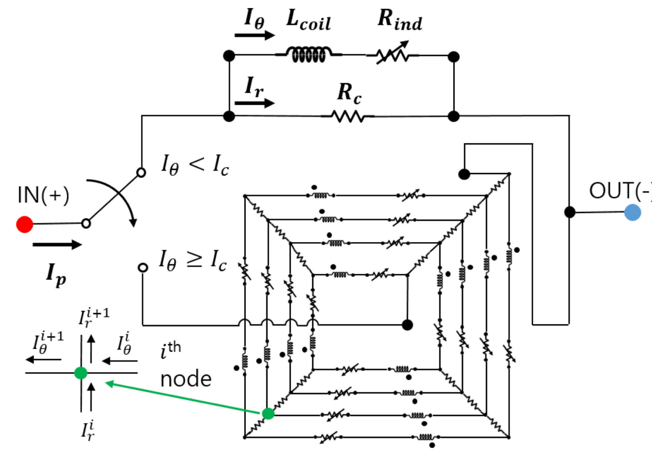

Fig. 2. Conceptual drawing for the combined circuit model. When the operating current I_θ in Fig. 1(a) is smaller than the coil's critical current I_c, the lumped circuit model is selected, while $I_\theta \geq I_c$, the distributed network model. In this figure, the "intermediate" moment is set to be at $I_\theta = I_c$, though any moments at $I_\theta < I_c$ may be selected as the intermediate moment conservatively.

inductance of the coil; (2) a parallel resistor R_c, often called "characteristic resistance", that represents the radial current path through turn-to-turn contacts; and (3) a series resistor R_{ind}, the index resistance. R_c of an N-turn NI pancake coil may be estimated by equation (1):

$$R_c = \sum_{i=1}^{N} \frac{R_{ct}}{2\pi r_i w_d}, \tag{1}$$

where R_{ct}, r_i, and w_d are, respectively, average turn-to-turn contact resistivity (unit: $\Omega\cdot\text{m}^2$), radius of the i^{th} turn, and HTS tape width[26]. R_{ind} may be expressed by equation (2)[27]:

$$R_{ind} = \frac{E_c l}{I_\theta} \left(\frac{I_\theta}{I_c}\right)^n, \tag{2}$$

where E_c, I_c and l are, respectively, critical electric field of 1 μV/cm, critical current, and tape length of the coil. I_p, I_θ, and I_r are defined in Fig. 1 as power supply current, azimuthal current that generates axial magnetic field, and radial leak current through the turn-to-turn contacts, respectively. In the lumped circuit simulation, precise modeling of R_c and R_{ind} as a function of temperature, operating current, and magnetic field is crucial to improve the simulation accuracy. Lu *et al.*, reported an in-depth study on correlation between R_c and turn-to-turn contact resistance [28]. Kim *et al.*, reported an experimental study on effects of winding tension on R_c and R_{ct} [29]. Recently, Noguchi *et al.*, reported a significant impact of the Hall effect on the terminal voltage of an NI coil due to the turn-to-turn radial current (I_r in Fig. 1) under a large external magnetic field [30].

B. Conventional Approach #2: Distributed Network Model

The distributed model in Fig. 1(b) discretizes an NI coil into multiple subcoil segments based on the partial element equivalent circuit (PEEC) technique [19]. Electrical components for each segment are similar to those in the lumped model: (a) L^i_{coil} for inductance of the i^{th} coil; (b) R^i_c characteristic resistance; and (c) R^i_{ind} index resistance. Using the distributed model, Yanagisawa *et al.*, proposed the *single-turn-to-multi-turn* transition concept for the first time to explain the well-known "current sharing" feature of an NI coil [17]. Since then, multiple groups explored the distributed network approach [17]–[21]. However, the distributed network simulation of an "actual" NI HTS magnet and their comparison with experiment has not been reported yet. The excessive calculation time may be a primary reason for the limited efforts on the distributed model simulation in a magnet level [24], [25].

III. Combined Model: A Combination of Lumped Circuit and Distributed Network Models

A. Key Idea: Selective Use of Either Lumped or Distributed

Imagine an NI coil being charged beyond its critical current. When the operating current of the coil (I_θ in Fig. 1(a)) is small and below the critical current I_c, the radial leak current (I_r in Fig. 1(a)) may be assumed to be uniform in the coil, because electromagnetic diffusion of the coil current in the azimuthal direction is substantially faster than that in the radial direction due to the turn-to-turn contact resistance [24]. Thus, the lumped circuit model may suffice to analyze the NI behaviors. When the coil current increases beyond the critical current, the distributed model takes over the role to simulate the spatially distributed currents, both radial and azimuthal. The key concept of the combined model is illustrated in Fig. 2, i.e., the lumped circuit model is selected when $I_\theta < I_c$, while the distributed network model is selected when $I_\theta \geq I_c$. In Fig. 2, the "intermediate" moment is set to be at $I_\theta = I_c$, though any moments at $I_\theta < I_c$ may be selected as the intermediate moment conservatively.

B. Equal Power Constraint at "Intermediate" Moment In Transition from Lumped Model to Distributed Model

Until the "intermediate" moment (at $I_\theta = I_c$ in case of Fig. 2), both radial (I_r) and azimuthal (I_θ) currents in the NI coil are

TABLE I
AN NI HTS TEST COIL FOR "OVER-CURRENT" TEST AND SIMULATION

Parameters		Values
HTS Wire		Super Power SCS4050
Wire width; thickness	[mm]	4.0; 0.1
Copper stabilizer thickness	[mm]	0.04
I_c at 77 [K], self-field	[A]	85
I_c at 77 [K], coil	[A]	63
Insulation		No-insulation (NI)
Number of turns		30
Coil I.D.; O.D.	[mm]	60; 66
Coil height	[mm]	4.0
Coil constant	[Gauss/A]	6.0
Inductance, L_{coil}	[μH]	110.0
Surface contact resistance, R_{ct}	[$\mu\Omega\cdot$cm^2]	70
Characteristic resistance, R_c	[$\mu\Omega\cdot$cm^2]	359

assumed to be spatially uniform in the lumped model. However, when the distributed network model comes into play at the intermediate state, the initial currents in all segments, radial (I_r^i) and azimuthal (I_θ^i) in Fig. 2, must be defined. Here, we propose an *equal power constraint* at the intermediate moment, i.e., the total Ohmic power dissipation in the lumped model ($I_r^2 R_c$) equals that in the distributed model ($\sum {I_r^i}^2 R_c^i$). Then, an effective average radial current of I_r^{ep} may be defined as equation (3) and I_r^i in all segments is assumed to be constant and equal to I_r^{ep}. Then, I_θ^i at each segment in the distributed model may be obtained by applying the Kirchhoff's current law. Note that the power supply current of I_p in the lumped model remains the same in the distributed model, which plays the boundary conditions at the coil terminals, IN and OUT in Fig. 2, at the intermediate state.

$$I_r^{ep} = \sqrt{\frac{I_r^2 R_c}{\sum_{i=1}^{N} (R_c^i)^2}} \tag{3}$$

IV. CASE STUDY: AN 30-TURN NI REBCO TEST COIL

A. *Coil Specification and Summary on Experimental Results*

A 30-turn single-pancake NI test coil was wound with 4 mm wide and 0.1 mm thick REBCO tapes made by the Super Power, Inc. Key parameters of the coil are summarized in Table I. The coil was previously constructed and tested at the MIT Francis Bitter Magnet Laboratory [1]. In an "over-current" test, the coil was *intentionally* charged beyond its critical current of 63 A up to 120 A. Simulation results with the distributed model were previously reported in [19], which agreed well with the experimental ones. The test was performed in a bath of liquid nitrogen at 77 K.

B. *Simulation Results and Comparison*

First, we simulated the over-current test using the lumped, distributed, and combined models individually and compared them to each other as well as the experimental ones. In the combined model analysis, the intermediate moment is conservatively set to be at $t = 100$ s when $I_\theta < I_c$. Figures 3 and 4 show magnetic fields at the coil center and coil terminal voltages, respectively, where squares, circles, diamonds, and triangles stand for the results from experiment, distributed model, combined model, and lumped model, respectively. Stars in the figures represent the power supply current ramping at 0.5 A/s. In the lumped circuit analysis, R_c of 359 $\mu\Omega$ and n of 10 were used, which were obtained from a separate test of the coil. In Fig. 4, an excessive discrepancy in terminal voltages was observed between the experimental raw data (squares, previously reported in [1]) and all the simulated results, which is an extremely rare case when compared with previous simulations of other NI coils. To further explore this issue, we performed an *inverse calculation of terminal voltage*, which is a technique to estimate the terminal voltages of an NI coil from the measured magnetic fields at the coil center, the measured characteristic resistance of R_c, and the measured coil constant (unit: T/A) [31], [32]. The results are presented in Fig. 4 as hexagrams, which agree reasonably well with the simulated ones. Therefore, we tentatively concluded an error in voltage measurement (squares in Fig. 4) during the test.

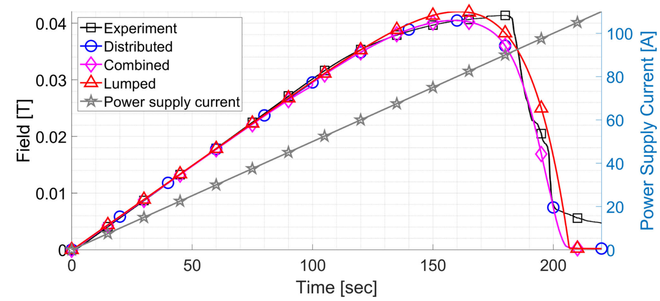

Fig. 3. Magnetic fields at the coil center vs. time: (a) squares from experiment; (b) circles from the distributed model; (c) diamonds from combined; and (d) triangles from lumped. Stars indicate the power supply current. The intermediate moment is conservatively set to be at $t = 100$ s when $I_\theta < I_c$.

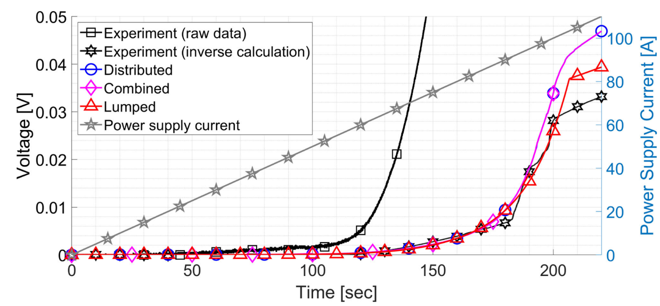

Fig. 4. Terminal voltages of the coil vs. time: (a) squares from experiment (raw data); (b) hexagrams from inverse calculation based on experimental results; (c) circles from the distributed model; (d) diamonds from combined ; and (e) triangles from lumped. Stars indicate the power supply current. The intermediate moment is conservatively set to be at $t = 100$ s when $I_\theta < I_c$.

In Fig. 3, magnetic fields of the lumped model show a notable difference from those of the distributed model, while the difference of magnetic fields between the distributed and combined models are barely discernible. In Fig. 4, the difference of terminal voltages between the distributed and combined models are also marginal, which demonstrates the validity of our combined model that generates essentially the identical results of the

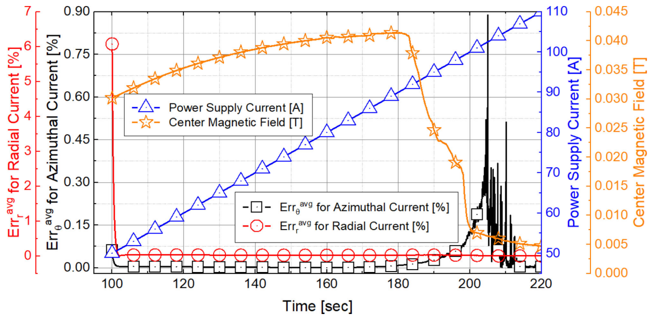

Fig. 5. Squares stand for $err_\theta^{avg}(t)$ in equation (5) representing the average absolute errors in percentile between the distributed and combined models for azimuthal currents in all segments; circles for $err_r^{avg}(t)$ in equation (4) representing radial. Triangles and stars stand for the respective power supply currents and magnetic fields at the center.

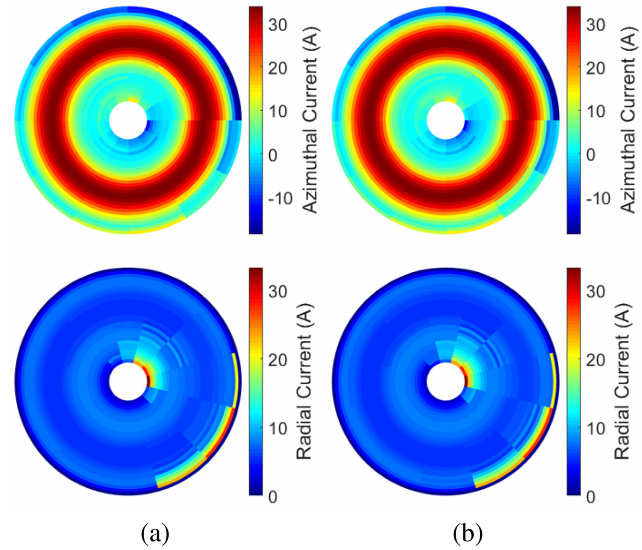

Fig. 6. Azimuthal (I_θ^i) and radial (I_r^i) currents in the NI coil at $t = 200$ s from: (a) the distributed model; and (b) the combined model.

distributed model. Note that the measured magnetic fields agree well with those of the combined model, while the measured terminal voltages, obtained from the inverse calculation that is based on the lumped circuit model, agree more to the results of the lumped circuit model. In the distributed model, field dependent critical currents $I_c(|B|, \theta)$ at 77 K of the SuperPower's REBCO tape, measured by a team led by D. Abraimov and curve-fit by Hilton *et al.* [33], at the National High Magnetic Field Laboratory were used to estimate $I_c(|B|, \theta)$ of each segment. The number of segments per each turn was limited to 12 in consideration of calculation time, as improvement in simulation accuracy with a larger number of segments was marginal.

C. Discussion

To quantitatively evaluate the discrepancy between the combined and distributed models, $err_r^{avg}(t)$ and $err_\theta^{avg}(t)$ are defined, respectively, by equations (4) and (5):

$$err_r^{avg}(t) = \frac{1}{N}\sum_{i=1}^{N}\left|1 - \frac{I_{r,comb}^i(t)}{I_{r,dist}^i(t)}\right| \tag{4}$$

$$err_\theta^{avg}(t) = \frac{1}{N}\sum_{i=1}^{N}\left|1 - \frac{I_{\theta,comb}^i(t)}{I_{\theta,dist}^i(t)}\right|, \tag{5}$$

where $I_{r,comb}^i(t)$ and $I_{\theta,comb}^i(t)$ are the respective radial and azimuthal currents of the i^{th} segment in the combined model, while $I_{r,dist}^i(t)$ and $I_{\theta,dist}^i(t)$ distributed. $err_r^{avg}(t)$ essentially represents the average absolute errors in percentile between the distributed and combined models for radial currents in all segment, while $err_\theta^{avg}(t)$ represents those for azimuthal currents. Fig. 5 plots $err_r^{avg}(t)$ (circles) and $err_\theta^{avg}(t)$ (squares) after the intermediate moment, i.e., $t > 100$ s. Due to the equal power constraint at the intermediate moment, $err_r^{avg}(t)$ is at its peak of 6.1% then immediately decreases to $< 0.1\%$. $err_\theta^{avg}(t)$ looks rapidly increasing after the NI coil experienced a "full" quench but still the peak of $err_\theta^{avg}(t)$ is less than 1%. The results well explain the good agreement in both magnetic fields and terminal voltages between the distributed and combined models in Figs. 3 and 4. Fig. 6 presents azimuthal and radial currents in the NI coil at $t = 200$ s from: (a) the distributed model; and (b) the combined model. The difference between the results from the two methods is essentially negligible.

V. Conclusion

We proposed a "combined" model to simulate the non-linear behaviors of a no-insulation (NI) high temperature superconductor (HTS) coil, essentially combination of the lumped circuit model and the distributed network model. The key idea is a selective use of the two models depending on an operating condition. When the azimuthal current of an NI coil is below its critical current, the lumped circuit model may suffice to analyze the non-linear NI behaviors. When the current surpasses the critical current, the distributed model takes over the role to simulate nonuniform spatial distributions of currents, both radial and azimuthal. The equal power constraint was proposed to determine the radial current distribution for the distributed model at the intermediate state, then the azimuthal currents are calculated by solving the distributed network circuit with the Kirchhoff's laws. To verify the combined model, the over-current test of a 30-turn NI REBCO single-pancake coil was simulated with the lumped, distributed, and combined models individually, and the results were compared to each other as well as the experimental ones. The simulation results of the combined model are barely discernible from those of the distributed model; they also show good agreement with the experimental ones. The results verify the validity of the combined circuit model for more efficient simulation of the NI behaviors than the distributed model. By limiting the use of the time-consuming distributed model only for the post-quench analysis, the combined model may substantially reduce the overall calculation time without sacrificing simulation accuracy.

References

[1] S. Hahn, D. K. Park, J. Bascuñán, and Y. Iwasa, "HTS pancake coils without turn-to-turn insulation," *IEEE Trans. Appl. Supercond.*, vol. 21, no. 3, pp. 1592–1595, Jun. 2011.

[2] S. Hahn *et al.*, "A 78-mm/7-T multi-width no-insulation ReBCO magnet: Key concept and magnet design," *IEEE Trans. Appl. Supercond.*, vol. 24, no. 3, Jun. 2014, Art. no. 4602705.

[3] J. Bascuñán, S. Hahn, T. Lecrevisse, J. Song, D. Miyagi, and Y. Iwasa, "An 800-MHz all-REBCO insert for the 1.3-GHz LTS/HTS NMR magnet program—A progress report," *IEEE Trans. Appl. Supercond.*, vol. 26, no. 4, Jun. 2016, Art. no. 4300205.

[4] D. Uglietti, R. Wesche, and P. Bruzzone, "Construction and test of a non-insulated insert coil using coated conductor tape," *J. Phys.*, vol. 507, no. 3, 2014, Art. no. 032052.

[5] J. Liu, Y. Dai, and L. Li, "Progress in the development of a 25 T all superconducting NMR magnet," *Cryogenics*, vol. 79, pp. 79–84, 2016.

[6] T. Lécrevisse and Y. Iwasa, "A (RE)BCO pancake winding with metal-as-insulation," *IEEE Trans. Appl. Supercond.*, vol. 26, no. 3, Apr. 2016, Art. no. 4700405.

[7] S. Hahn, D. K. Park, J. Voccio, J. Bascunan, and Y. Iwasa, "No-insulation (NI) HTS inserts for >1 GHz LTS/HTS NMR magnets," *IEEE Trans. Appl. Supercond.*, vol. 22, no. 3, Jun. 2012, Art. no. 4302405.

[8] J. Liu *et al.*, "Generation of 24 T with an all superconducting magnet," *IEEE/CSC ESAS Supercond. News Forum*, vol. 35, pp. STH39 (HP105), Jan. 2016.

[9] S. Yoon, J. Kim, K. Cheon, H. Lee, S. Hahn, and S.-H. Moon, "26 T 35 mm all-Gd $Ba_2Cu_3O_7$–x multi-width no-insulation superconducting magnet," *Supercond. Sci. Technol.*, vol. 29, no. 4, 2016, Art. no. 04LT04.

[10] J. Choi, S. Kim, S. Kim, K. Sim, M. Park, and I. Yu, "Characteristic analysis of a sample HTS magnet for design of a 300 kW HTS DC induction furnace," *IEEE Trans. Appl. Supercond.*, vol. 26, no. 3, Apr. 2016, Art. no. 3700405.

[11] S. Hahn *et al.*, "Construction and test of 7-T/68-mm cold-bore multiwidth no-insulation GdBCO magnet," *IEEE Trans. Appl. Supercond.*, vol. 25, no. 3, Jun. 2015, Art. no. 4600405.

[12] Y. Choi *et al.*, "The effects of partial insulation winding on the charge–discharge rate and magnetic field loss phenomena of GdBCO coated conductor coils," *Supercond. Sci. Technol.*, vol. 25, no. 10, 2012, Art. no. 105001.

[13] S. Hahn *et al.*, "No-insulation multi-width winding technique for high temperature superconducting magnet," *Appl. Phys. Lett.*, vol. 103, no. 17, 2013, Art. no. 173511.

[14] T. Painter *et al.*, "Design, construction and operation of a 13 T 52 mm no-insulation REBCO insert for a 20 T all-superconducting user magnet," presented at the 25th Int. Conf. Magnet Technol., Amsterdam, The Netherlands, 2017.

[15] J. Kim *et al.*, "Effect of resistive metal cladding of HTS tape on the characteristic of no-insulation coil," *IEEE Trans. Appl. Supercond.*, vol. 26, no. 4, Jun. 2016, Art. no. 4601906.

[16] Y. J. Hwang, J. Y. Jang, S. Song, J. M. Kim, and S. Lee, "Feasibility study of the impregnation of a no-insulation HTS coil using an electrically conductive epoxy," *IEEE Trans. Appl. Supercond.*, vol. 27, no. 4, Jun. 2017, Art. no. 4603405.

[17] Y. Yanagisawa *et al.*, "Basic mechanism of self-healing from thermal runaway for uninsulated REBCO pancake coils," *Physica C*, vol. 499, pp. 40–44, 2014.

[18] Y. Wang, H. Song, D. Xu, Z. Li, Z. Jin, and Z. Hong, "An equivalent circuit grid model for no-insulation HTS pancake coils," *Supercond. Sci. Technol.*, vol. 28, no. 4, 2015, Art. no. 045017.

[19] T. Wang *et al.*, "Analyses of transient behaviors of no-insulation REBCO pancake coils during sudden discharging and overcurrent," *IEEE Trans. Appl. Supercond.*, vol. 25, no. 3, Jun. 2015, Art. no. 4603409.

[20] Y. Wang, W. K. Chan, and J. Schwartz, "Self-protection mechanisms in no-insulation (RE) $Ba_2Cu_3O_x$ high temperature superconductor pancake coils," *Supercond. Sci. Technol.*, vol. 29, no. 4, 2016, Art. no. 045007.

[21] A. Ikeda *et al.*, "Transient behaviors of no-insulation REBCO pancake coil during local normal-state transition," *IEEE Trans. Appl. Supercond.*, vol. 26, no. 4, Jun. 2016, Art. no. 4600204.

[22] K. R. Bhattarai, K. Kim, S. Kim, S. Lee, and S. Hahn, "Quench analysis of a multiwidth no-insulation 7-T 78-mm REBCO magnet," *IEEE Trans. Appl. Supercond.*, vol. 27, no. 4, Jun. 2017, Art. no. 4603505.

[23] J. Y. Jang *et al.*, "Design, construction and 13 K conduction-cooled operation of a 3 T 100 mm stainless steel cladding all-REBCO magnet," *Supercond. Sci. Technol.*, vol. 30, no. 10, 2017, Art. no. 105012.

[24] W. D. Markiewicz, J. J. Jaroszynski, D. V. Abraimov, R. E. Joyner, and A. Khan, "Quench analysis of pancake wound REBCO coils with low resistance between turns," *Supercond. Sci. Technol.*, vol. 29, no. 2, 2015, Art. no. 025001.

[25] H. Song and Y. Wang, "Simulations of nonuniform behaviors of multiple no-insulation (RE) $Ba_2Cu_3O_{7-x}$ HTS pancake coils during charging and discharging," *IEEE Trans. Appl. Supercond.*, vol. 26, no. 4, Jun. 2016, Art. no. 4700105.

[26] X. Wang *et al.*, "Turn-to-turn contact characteristics for an equivalent circuit model of no-insulation ReBCO pancake coil," *Supercond. Sci. Technol.*, vol. 26, no. 3, 2013, Art. no. 035012.

[27] K. Yamafuji and T. Kiss, "Current-voltage characteristics near the glass-liquid transition in high-TC superconductors," *Physica C*, vol. 290, no. 1-2, pp. 9–22, 1997.

[28] J. Lu, J. Levitan, D. McRae, and R. P. Walsh, "Contact resistance between two REBCO tapes: The effects of cyclic loading and surface coating," *Supercond. Sci. Technol.*, vol. 31, no. 8, 2018, Art. no. 085006.

[29] K. L. Kim *et al.*, "Effect of winding tension on electrical behaviors of a no-insulation ReBCO pancake coil," *IEEE Trans. Appl. Supercond.*, vol. 24, no. 3, Jun. 2014, Art. no. 4600605.

[30] S. Noguchi, K. Kim, and S. Hahn, "Simulation on electrical field generation by hall effect in no-insulation REBCO pancake coils," *IEEE Trans. Appl. Supercond.*, vol. 28, no. 3, Apr. 2018, Art. no. 4901805.

[31] J. B. Song and S. Y. Hahn, "'Leak current' correction for critical current measurement of no-insulation HTS coil," *Prog. Supercond. Cryogenics*, vol. 19, no. 2, pp. 48–52, 2017.

[32] S. Hahn *et al.*, "No-insulation coil under time-varying condition: Magnetic coupling with external coil," *IEEE Trans. Appl. Supercond.*, vol. 23, no. 3, Jun. 2013, Art. no. 4601705.

[33] D. Hilton, A. Gavrilin, and U. Trociewitz, "Practical fit functions for transport critical current versus field magnitude and angle data from (RE)BCO coated conductors at fixed low temperatures and in high magnetic fields," *Supercond. Sci. Technol.*, vol. 28, no. 7, 2015, Art. no. 074002.